# Monitoring of long-span bridge deformation based on 3D laser scanning

**Xi Chu*, Zhixiang Zhou, Xiaoju Xiang , Songlin He, Xu Hou**

*Dept. of State Key Laboratory Breeding Base of Mountain Bridge Tunnel Engineering, Chongqing Jiaotong University Chongqing 400074, China*
*jfnchuxi@yahoo.com*

ABSTRACT. *This paper applies the 3D ground laser scanning technique to monitor the high-temperature deformation of a long-span steel truss arch bridge, whose main span is 432m in length. Under the daily temperature difference of 9ºC, the three dimensions of the bridge was scanned twice by laser, and the collected data was pre-processed for further analysis. After that, a new deformation measurement method for the non-uniform rational basis spline (NURBS) surface was put forward based on 3D point cloud data, and adopted to measure the overall deformation of the said bridge. The measured results were compared to those captured by the precision level and the total station, indicating that the proposed 3D laser scanning system and data processing method enjoy good accuracy and reliability. Compared with the traditional single-point deformation monitoring methods, our method can record the linear deformation and present the overall deformation features. The proposed method boasts good prospects in engineering application.*

RÉSUMÉ. *Cet article applique la technique de balayage laser 3D au sol pour surveiller la déformation à haute température d'un pont des poutres treillis en arc à longue portée, dont la longueur de la portée principale est de 432 m. Sous la différence de température quotidienne de 9 ºC, les trois dimensions du pont ont été scannées deux fois au laser et les données collectées ont été prétraitées pour une analyse plus approfondie. Après cela, une nouvelle méthode de mesure de la déformation de la surface des B-splines rationnelles non uniformes (NURBS, le sigle de « Non-Uniform Rational Basis Splines » en anglais) a été proposée sur la base de données de nuages de points 3D, et adoptée pour mesurer la déformation globale pont cible. Les résultats mesurés ont été comparés à ceux capturés par le niveau de précision et la station totale, indiquant que le système de balayage laser 3D et le procédé de traitement de données proposés bénéficient d'une bonne précision et d'une grande fiabilité. Comparée aux méthodes traditionnelles de surveillance de la déformation en un seul point, notre méthode peut enregistrer la déformation linéaire et présenter les caractéristiques de déformation globales. La méthode proposée présente de belles perspectives d'application technique.*

KEYWORDS: *deformation monitoring, ground-based 3D, laser scanning, nurbs surfaces, point cloud precision.*

MOTS-CLÉS: *surveillance de déformation, 3D sur la base de terre, balayage laser, Surfaces de banlieue, précision des nuages de points.*

DOI:10.3166/I2M.17.113-130 

## 1. Introduction

The safety state of bridge structure depends on the relative deformation of the bridge. Therefore, accurate measurement of the deformation of bridge structure is an important part of the research field of bridge health monitoring. In the conventional deformation monitoring of long-span bridges, the shape change of bridges is mainly obtained through the deployment of sensors at limited structural key points, or only through theodolites, levelers, total station and other equipment to measure the deformation value of limited points. The disadvantage of this method lies in the large workload in the field, the location of the points is limited by the topographic conditions, and only limited deformation data of individual points are obtained, while the deformation information of the whole bridge is difficult to obtain. Ground three-dimensional laser scanning technology is a kind of measuring technology which can quickly acquire a large number of three-dimensional coordinates of measuring points by means of laser ranging. This technology can overcome the limitations of traditional measuring technology and obtain the overall deformation information of structures. At present, many studies have focused on the application of ground three-dimensional laser scanning technology in Bridge engineering (Zeng *et al*., 2015; Zawieska *et al*., 2015; Zhou *et al*., 2011; Cristea *et al*., 2015). However, most of the research focuses on the feasibility of three-dimensional laser scanning in bridge deformation monitoring. Most of the purpose is to obtain the three-dimensional model of the bridge. However, the relative deformation measurement of long-span bridges using three-dimensional laser scanning technology on the ground has not yet been formally reported in the literature. To measure the relative deformations of bridges by using three-dimensional laser scanning technology on the ground, two problems need to be solved: a reasonable on-site testing scheme should be formulated for the super-long linear structure of bridges to take into account the accuracy and efficiency of data acquisition; on the other hand, because the original data of three-dimensional laser scanning on the ground cannot directly reflect the relative deformation of the bridge, it is necessary to find a suitable data processing method. In this paper, the relative deformation measurement method of long-span steel truss deck arch bridge with 432m main span is studied from two aspects of data acquisition and data processing. The reliability of this method in relative deformation measurement of bridges is verified based on the measurement results of precision level and total station. This method makes up for the shortcomings of conventional deformation measurement methods which lack the overall deformation characteristics of bridges, and has good engineering application prospects.

## 2. Literature review

In recent years, many researchers have focused on the application of ground-based three-dimensional laser scanning technology in bridge engineering. Riveiro *et al*. (2011) obtained the 3D shape of a stone arch bridge which is a world heritage by static three-dimensional laser scanning system, and evaluated the critical load which was supported by numerical simulation analysis. Aimed at the deformation

monitoring for ancient arch bridges, Soni *et al*. (2015) processed the point cloud data by nonparametric statistics in the absence of any design parameters, to obtain precise geometric dimensions of arch, and analyzed the arch deformation. Chen *et al*. (2010) applied the three-dimensional laser scanning technology to the deformation monitoring of the main forced members of the bridge, which ensured the timely and precise acquirement of the space deformation information of bridge components. Their achievements are referred by policy makers to formulate preventive measures for disasters. The above research mainly focused on the feasibility of three-dimensional laser scanning in bridge deformation monitoring by establishing the 3D model of bridge. In contrast, the measurement of relative deformation of large span bridge by ground-based three-dimensional laser scanning technology has not been officially reported in existing literature.

Taking the long span steel truss arch bridge with the main span of 432m as the research object, this paper analyzes the ways to measure the relative deformation of large span bridge by the ground-based three-dimensional laser scanning technology in two aspects of data acquisition and data processing. In addition, the reliability of the method in measuring the relative deformation of bridge is verified by taking the measurement results of precision level and total station as the standard.

## 3. Methods

### *3.1. Application of three-dimensional laser scanning in large span bridge displacement monitoring*

#### *3.1.1. Basic principle of three-dimensional laser scanning*

The scanning oblique distance r from the station to the scanning point can be obtained by three-dimensional laser scanning. According to the horizontal angle φ and vertical angle θ of the scanning point, the relative coordinate difference in the three-dimensional space between each scanning point and the measurement station is further calculated (Du and Teng, 2007). The scanners an approximate square. The y scanning axis is parallel to the sidewall of the host, x axis is vertical to the sidewall, and z axis is vertical to the subface of the instrument. In the local coordinate system within the scanner (Figure 1), the three-dimensional coordinates of any scanning point O can be represented as (Nurunnabi *et al*., 2016).

$$\begin{cases} x = r\cos\varphi\cos\theta \\ y = r\sin\varphi\cos\theta \\ z = r\sin\varphi \end{cases} \tag{1}$$

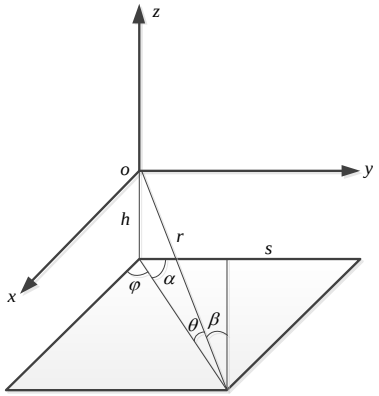


*Figure 1. Geometric relation of laser scanning*

The most direct measurement data obtained by three-dimensional laser scanning is the 3D coordinates of a single scanning point. Therefore, the variance of space coordinate is used as the evaluation index of the precision of point cloud data. Formula (1) is conducted with Taylor series expansion, and the quadratic term and above are omitted. Under the covariance propagation law, the variance-covariance matrix of three-dimensional coordinates is obtained based on the linear expression of the function (Battauz *et al*., 2011).

$$D_{uu} = \begin{pmatrix} \sigma_x^2 & \sigma_{xy} & \sigma_{xz} \\ \sigma_{yx} & \sigma_y^2 & \sigma_{yz} \\ \sigma_{zx} & a_{zy} & \sigma_z^2 \end{pmatrix} = \begin{pmatrix} \sigma_r^2 & 0 & 0 \\ 0 & \sigma_\varphi^2 & 0 \\ 0 & 0 & \sigma_\theta^2 \end{pmatrix} u_{i'j}^T \tag{2}$$

The partial derivatives of the items in formula (1) are calculated.

$$u_{i'j} = \begin{pmatrix} \cos\varphi\cos\theta & -r\sin\varphi\cos\theta & -r\cos\varphi\sin\theta \\ \sin\varphi\cos\theta & r\cos\varphi\cos\theta & -r\sin\varphi\sin\theta \\ \sin\theta & 0 & r\cos\theta \end{pmatrix} \tag{3}$$

The variance components of the point cloud data in the directions of x, y and z are:

$$\begin{cases} \sigma_x^2 = (\cos\varphi\cos\theta)^2\sigma_r^2 + (r\sin\varphi\cos\theta)^2\sigma_\varphi^2 + (r\cos\varphi\sin\theta)^2\sigma_\theta^2 \\ \sigma_y^2 = (\sin\varphi\cos\theta)^2\sigma_r^2 + (r\cos\varphi\cos\theta)^2\sigma_\varphi^2 + (r\sin\varphi\sin\theta)^2\sigma_\theta^2 \\ \sigma_z^2 = (\sin\theta)^2\sigma_r^2 + (r\cos\theta)^2\sigma_\varphi^2 \end{cases} \tag{4}$$

In theory, the variance of single point spatial coordinates of point cloud data is:

$$\sigma_p^2 = \sigma_x^2 + \sigma_y^2 + \sigma_z^2 = \sigma_r^2 + r^2 \cos^2\theta\sigma_\varphi^2 + r^2\sigma_\theta^2 = \sigma_r^2 + r^2 \sin^2\beta\sigma_\varphi^2 + r^2\sigma_\theta^2 \quad (5)$$

where the vertical scanning angle β=90º-θ is the included angle between the incident laser and the surface normal line of the target point (Figure 1). σr is ranging accuracy, σφ is horizontal angle measuring accuracy, and σθ is vertical angular measuring accuracy.

According to the above error evaluation model, the point accuracy of single scanning point in the measuring station can be evaluated. Taking the RIEGL VZ-1000 three-dimensional laser scanner used in bridge test in this paper as an example (σr=2mm, at the distance of 1,000m, σφ and σθ are 8.73×10-6rad), the cloud chart of the point position accuracy in the station is obtained (Figure 2).

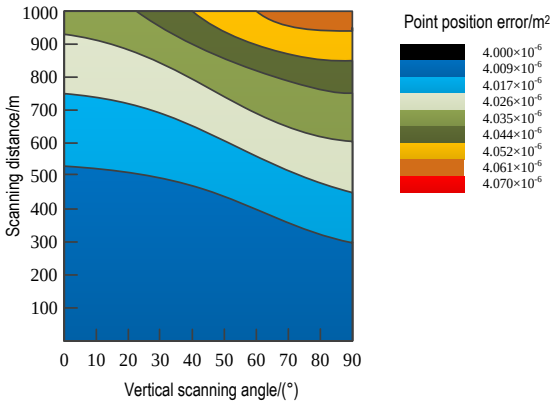


*Figure 2. Single point position error*

Formula 5 and Figure 2 indicate that the position accuracy of a single scanning point is affected by the working angle $\theta$ and the scanning slope distance r of laser scanner. According to $\sigma_r$, $\sigma_\varphi$, $\sigma_\theta$, $r$ and the vertical angle $\theta$ of the scanner, the variance of the space coordinates of a single scanning point can be obtained. Therefore, the laser scanned point cloud data of different points of large span bridges also have different point positioning accuracies. When the scanning distance $r$ and the vertical scanning angle $\theta$ is small, smaller laser spot means stronger echo signal and more accurate measurement. Otherwise, the measurement accuracy decreases. When the scanning distance and the vertical scanning angle continuously increase, the instrument will not collect enough echo information, resulting in the failure of the measurement. Therefore, in the process of three-dimensional laser scanning deformation monitoring for long-span bridges, it is particularly important to evaluate the accuracy of the point cloud scanned in the station by using the above-mentioned error model.

On the other hand, for three-dimensional laser scanning of long span bridges, we should test not only the precision of the spatial position of a single point, but also

pay attention to the resolution of point cloud data on bridge surface. High resolution point cloud data is the prerequisite to extract the geometrical outline and detailed deformation features of the object. The plane resolution is mainly related to two factors: the density of the point cloud and the size of the spot on the object surface. Higher plane point density and smaller spot size can achieve higher plane resolution (Gonzálezferreiroc *et al*., 2013). Leonidopoulos (2016) derived the theoretical formula for calculating the density of point cloud, and verified the relation between the density of point cloud and scanning distance and scanning angle by scanning experiment. The scanning distance is *s*, and the density of the point cloud on the facade is:

$$N_v = N_x N_z = \frac{\cos^3\alpha\cos^2\theta}{s^2 d\alpha d\theta} \tag{6}$$

on the horizontal surface, the density of the point cloud data is:

$$N_h = \frac{h\cos^3\alpha}{(sh^2\cos^3\alpha + s^3)d\alpha d\theta} \tag{7}$$

where $\alpha$=90º-$\varphi$ is defined as the horizontal scanning angle (see Figure 1). $d\alpha$ and $d\theta$ are constants representing the respective vertical and horizontal angular step frequency of the scanner. For RIEGL VZ-1000 three-dimensional laser scanner, the constant is $d\alpha$=$d\theta$-0.0024º. *h* is the height of the instrument.

Figure (3a) shows the data density map of the point cloud in the facade calculated by formula (6) when the vertical angle is equal to 0. The point cloud data density map on the vertical plane Figure (3a) and formula (6) shows that the surface density of the point cloud data on the vertical plane drops rapidly with the increase of the scanning distance, inversely proportional to the square of the distance. As the vertical scanning angle increases, the surface density of the point cloud data decreases and is proportional to the square of the cosine of angle in vertical direction. With the increase of the horizontal scanning angle, the surface density of the point cloud data decreases and is proportional to the three powder of the cosine. Figure (3b) is the data density map of the point cloud on the horizontal plane calculated by formula (7) in different scanning distances and at different horizontal scanning angles. According to Formula (7) and the point cloud data density map on the horizontal plane in Figure (3a), the density of point cloud data on the horizontal plane decreases sharply with the scanning distance. The change rate of point cloud density with scanning distance is greater on the horizontal plane than on the vertical plane. The change rate of point cloud density with scanning angle is smaller on the horizontal plane than on the vertical plane.

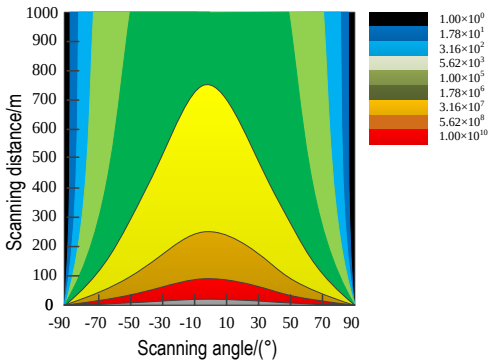


(a) Nephogram of point cloud density in vertical plan

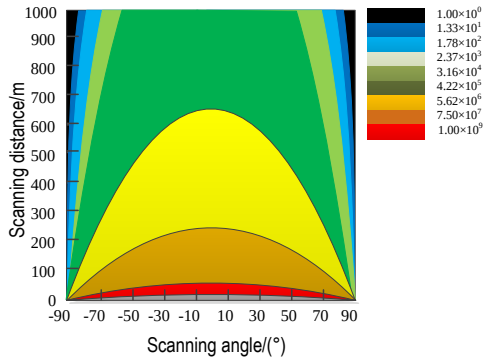


(b) Nephogram of point cloud density in horizontal plan

*Figure 3. Density figure of point cloud*

Based on the above analysis, as the accuracy of three-dimensional laser scanning of large span bridges varies with how dense the point cloud is, scanning stations should be installed on both the vertical and the horizontal surface of the bridge. Formula (6) of point cloud data density on the vertical plane is suitable for the analysis of the vertical load bearing components in the lower part of the bridge model, such as column, arch ring, and suspension cable. Formula (7) of point cloud data density on the horizontal plane is suitable for the analysis of the horizontal load bearing components in the upper part of the bridge model, such as bridge deck and bridge slab.

### *3.1.2. Three-dimensional laser scanning strategy of Daning River Bridge*

Based on the above discussion, when three-dimensional laser scanning technology is applied to monitor the deformation of large span bridges, the density

and accuracy of the point cloud are different in the spatial location of the bridge. Therefore, in actual measurement, the horizontal scanning angle, vertical scanning angle, and scanning distance should be comprehensively determined according to the scanning field of view of the three-dimensional laser scanner, the actual size of the bridge and the topographic features. The technical details of scanning should be reasonably designed to obtain higher point cloud density and spatial position accuracy. To ensure the high accuracy of spatial coordinates of a single scanning point, it is necessary to maintain as small the scanning slant distance as possible and control the range of scanning angle in a way that enabling the instrument to record enough echo information. As can be seen from the point cloud density map, the point cloud density is higher when S is within the range of 500m-600m and the scanning angle is [-30º, 30º]. If the scanning distance increases, the density of the plane point will decrease, a large amount of detail information will be lost and the spot size will increase, reducing the accuracy of single point space coordinate.

Daning River Bridge is located in the mountain valley terrain, with the relative height difference of 228m, having great depth of excavation and severe topographic relief. The main span of the bridge is 432m, ranking top in Asia and second in the world. Compared with the conventional three-dimensional laser scanning structure, this bridge has harsher field measuring conditions, fewer optional positions for measurement points, and larger scanning blind area. Therefore, the location of the scanning stations of the bridge needs to be rationally designed. Taking into account the scanning parameters of RIEGL VZ-1000, the single point error and point cloud density of laser scanning, and field measurement conditions, we determine to arrange three stations at such scanning angels: Station 1 [-17.2º,16.4º], Station 2 [-16.1º,17.3º], and Station 3 [-19.6º,15.7º], the farthest scan radius being set to 600m. Under the scanning scheme, the theoretical coverage of the high density point cloud on the side face of the bridge≥87.3%, and the theoretical coverage of the high density point cloud on the bridge deck ≥91.5%. The scanning point position and the density of the point cloud in the scanning area are shown in Figure 4, and the side elevation of the bridge is shown in Figure 5.

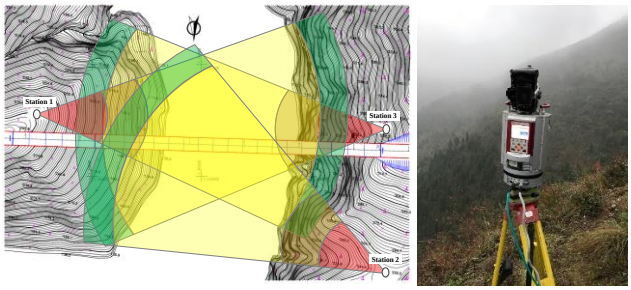


*Figure 4. Layout of measuring points and distribution of accuracy*

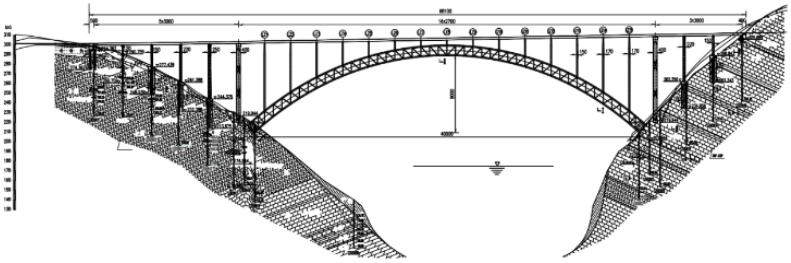

*Figure 5. Side elevation of the bridge*

The three-dimensional laser scanning is conducted at 4:00 and 14:00 (GMT+8) in winter. During this period, the environmental temperature difference of the bridge is 12°C, and the actual temperature rise of steel truss is 9.3°C. According to the above scanning scheme, the three-dimensional laser scanning results of Daning River Bridge are shown in Figure 6.

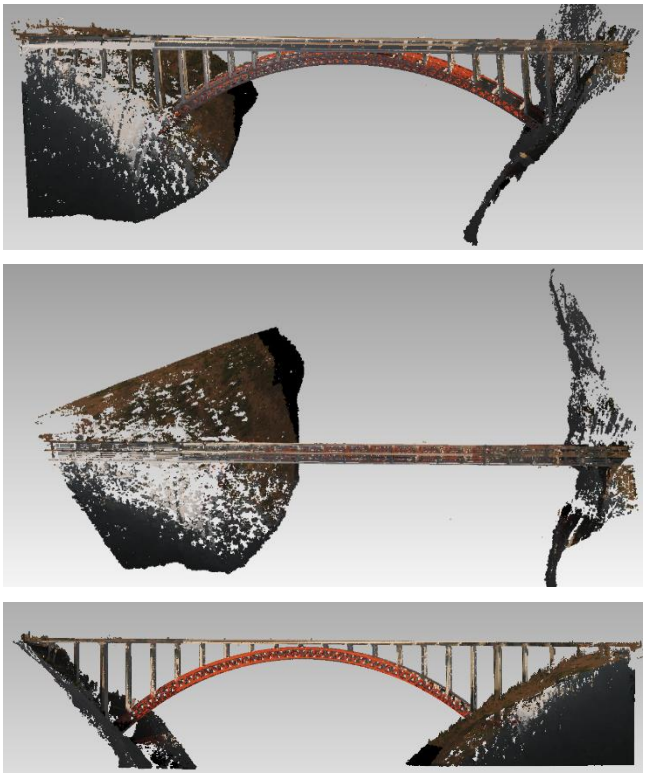

*Figure 6. 3D laser scanning results of Daning River Bridge*

### *3.2. Measurement of overall deformation of Daning River Bridge under temperature rise based on nurbs surface reconstruction*

NURBS surface is defined as (Bergström, 2015):

$$P(u,w)=\frac{\sum_{i=1}^{n}\sum_{j=0}^{m}B_{i,k}(u)B_{j,l}(u)W_{i,j}V_{i,j}}{\sum_{i=1}^{n}\sum_{j=0}^{m}B_{i,k}(u)B_{j,l}(u)W_{i,j}} \quad u\in[0,1] \tag{8}$$

where $V_{i,j}$($i$=0, 1, 2, …, $n$; $j$=0, 1, 2, …, $m$) is the position vector of vertices for a given feature grid (Zhang and Sun, 2016), and $W_{i,j}$ is the weighting factors for corresponding vertices. The recursion formula of base function is:

$$B_{i,o}(u)=\begin{cases}1, & u_i\le u\le u_{i+1}\\ 0, & \text{otherwise}\end{cases} \tag{9}$$

$$B_{i,k}(u)=\frac{u-u_i}{u_{i+k}-u_i}B_{i,k-1}(u)+\frac{u_{i+k+1}-u}{u_{i+k+1}-u_{i+1}}B_{i+1,k-1}(u),k\ge 1 \tag{10}$$

There is $k$+1 same nodes on both ends of the node vector, so that the curve can be tangent to the first and last sides by controlling the first and last ends of the polygon. The node vectors are:

$$U=[u_0\ \ u_0\ \ \cdots\ u_k\ \ u_{k+1}\ \cdots\ u_{r-k-1}\ \ u_{r-k}\ \ u_{r-k+1}\ \ \cdots\ u_r] \tag{11}$$

$$W=[w_0\ \ w_1\ \ \cdots\ w_l\ \ w_{l+1}\ \ \cdots\ w_{s-l-1}\ \ w_{s-l}\ \ w_{s-l+1}\ \ \cdots\ w_s] \tag{12}$$

$$\begin{aligned}&u_0=u_1=\cdots=u_k=0;\\ &u_{r-k}=u_{r-k+1}=\cdots=u_r=1;\\ &w_0=w_1=\cdots w_l=0;\\ &w_{s-l}=w_{s-l+1}=\cdots w_s=1\end{aligned} \tag{13}$$

The NURBS surface expresses the standard analytic shapes and freeform surface exactly by a unified expression. It can not only adjust the control vertex, but also make use of the weight factor, plus with stable calculation and geometric invariance in the linear transformation. By using this property, this paper proposes a deformation measurement method based on NURBS surface control points to measure the deformation of the surface in large visual field.

NURBS surface before deformation is taken as the original surface $S_0(u, v)$. The surface after deformation is $S(u, v)$, and the defined interval is still $u\in[0,1]$. Before deformation, proper synthetic functions should be constructed. In this paper, the

original synthetic functions of Cao En surfaces are transformed. In principle, the key points in Cao En surface have different synthetic functions. For simplicity, parameter $q_i$ is introduced for each key point, and the original form of the synthetic function is (Wyvill *et al*., 1992):

$$F_i(s) = \mathrm{e}^{[q_i(s-1)]} \tag{14}$$

where independent variable s is dot product $x.w_i$, and e is a constant. $t$ is the unit vector of the source point on the unit sphere, and $K_i(0 \le i \le n)$ are key points on the sphere. Let $p_i(0 \le i \le n)$ be the control point on the unit sphere, then the equation of the Cao En surface is:

$$S(t) = \frac{\sum_{i=0}^{n} p_i F_i(t, K_i)}{\sum_{i=0}^{n} F_i(t, K_i)} \tag{15}$$

Key point $K_i$ and the relevant synthetic function $F_i$ are interference terms of local deformation. Surface $S(t)$ after deformation is the sum of the weighted vector of all control points.

By substituting equation (15) to equation (14), the new form of the synthetic function is:

$$F_i(t, K_i) = \mathrm{e}^{[q_i(t.K_i - 1)]} \tag{16}$$

where $t.K_i$ is the dot product of two vectors. $q_i$ is a constant that adjusts the local influence of points. If $q_i$ is large, with the increase of the distance between the controlling point and the key point $K_i$, the influence of control points on synthetic surfaces can be rapidly reduced. In order to effectively process a large number of key points of NURBS surfaces based on point cloud data, the surface synthetic function is improved as follows:

$$F_i(t, w_i, r_i) = \begin{cases} C\left[\dfrac{(u - |K_i|)^2}{r_i^2}\right] & (u - |K_i|)^2 < r_i^2 \\ 0 & (u - |K_i|)^2 \ge r_i^2 \end{cases} \tag{17}$$

$C(x)=(1-x^2)^3$, is a polynomial function. When $x=1$, its value decreases to 0. $r_i$ is the influence radius. The function value of the points in the circle with radius $r_i$ is non-zero, while the function value of the points outside the circle is 0. Therefore, $F_i$ determines the local influence of control points on the surface.

Based on formula (17), the synthetic function $F_i$ of NURBS surface deformation in $u$, $v$ parameter space is improved as follows:

$$F_i(u,v,u_i,v_i,r_i) = C(\frac{d}{r_i}) = \begin{cases} \left[1-\left(\frac{d}{r_i}\right)^2\right]^3 & d \le r_i \\ 0 & d > r \end{cases} \quad (18)$$

where $d=\sqrt{[(u-u_i)^2+(v-v_i)^2]}$, and $d$ is the distance between any point ($u$, $v$) and key point ($u_i$, $v_i$) on $u$, $v$ parameter space surface. $F_i$ is utilized to determine the local influence of the control vector. When $d>r_i$, its value sharply decreases to 0. This indicates that the farther the control vector is away from the key point, the less it affects the synthesis surface. The surface model is shown in Figure 7.

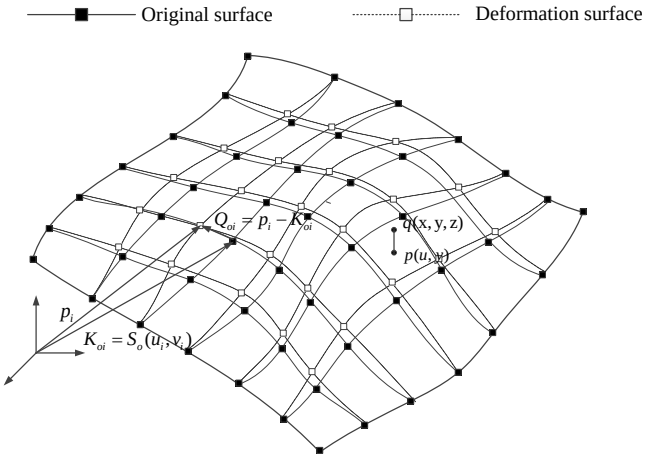


*Figure 7. Surface deformation model*

$K_{0i}$ is the key points on NURBS original surface in $u$, $v$ parameter space, and $K_{0i}=S_0(u_i, v_i)$, $0\le i\le n$. Each key point is related to the synthesis function $F_i(u, v, u_i, v_i, r_i)$. The position of the control vector is represented by $p_i$, and the control vector $Q_{oi}$ is:

$$Q_{oi} = p_i - K_{oi} \quad (19)$$

According to the Cao En surface equation (15), the deformation of the entire original surface can be expressed as:

$$D(u,v) = \frac{\sum_{i=0}^{n} Q_{0i} F_i(u,v,u_i,v_i,r_i)}{\sum_{i=0}^{n} F_i(u,v,u_i,v_i,r_i)} = \sum_{i=0}^{n} Q_{0i} f_i(u,v,u_i,v_i,r_i) \quad (20)$$

where $f_i(u,v,u_i,v_i,r_i)$ is the base function, and the expression is:

$$f_i(u,v,u_i,v_i,r_i)=\frac{F_i(u,v,u_i,v_i,r_i)}{\sum_{i=0}^{n}F_i(u,v,u_i,v_i,r_i)} \tag{21}$$

$D(u,v)$ is called displacement function, which is the weight sum of the control vector $Q_{oi}$ of each key point, representing the size of the original surface deformation caused by local deformation.

The base function $f_i$ can be converted from the synthesis function $F_i$. According to formula (20), the displacement function $D$ ($u$, $v$) can be regarded as a linear combination of base functions. By calculating the displacement function of the control vector of each key point on the NURBS primitive surface based on the point cloud data of the bridge, the local shape change of the surface deformation of the bridge can be obtained. Based on the above algorithm, the deformation of point cloud data of large span bridges obtained by three-dimensional laser scanning can be measured.

By using the method mentioned above, the point cloud data before and after the temperature rise of Daning river bridge is analyzed. The local shape change of the bridge deck is the deformation value of the bridge deck under the temperature effect. According to the value of the displacement function, the bridge deck deformation chromatogram is shown in Figure 8. Between the two expansion joints is the deformation chromatography of the main bridge deck, and outside of the expansion joint is the deformation chromatography of the approach slab. In the diagram, the legend on the right shows the degrees of deformation varying with different colors. In the midspan of the main bridge, the deformation values of the 9 points are extracted evenly. The deformation values of the midspan are 46.4mm-47.2mm of the left bridge deck and 45.7mm-46.5mm of the right bridge deck. The midspan deformation value obtained by the precision level is 44.6mm and 43.6mm. and the comparison results of the two measurements are shown in Table 1, indicating that the deformation values measured by the three-dimensional laser scanning system and the precision leveling measurement have a difference of less than 3mm, which means high accuracy.

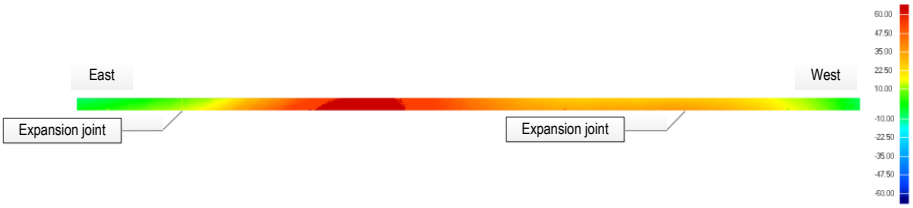


(a) Left side of bridge deck

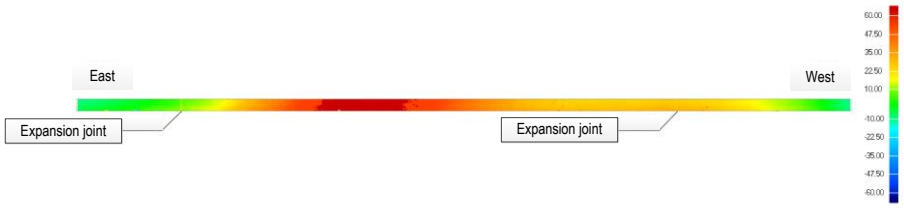


(b) Right side of bridge deck

*Figure 8. Bridge deck deformation chromatogram*

*Table 1. Mid-span deformation value*

| Bridge deck | Integral deformation measurement/mm | | | | | | | | |
|---|---|---|---|---|---|---|---|---|---|
| Left pavement | 46.4 | 46.8 | 47.1 | 47.2 | 46.5 | 46.7 | 46.6 | 46.7 | 46.5 |
| Error | 1.8 | 2.1 | 2.5 | 2.6 | 1.8 | 2.1 | 2.0 | 2.0 | 1.9 |
| Right pavement | 45.7 | 46.2 | 45.8 | 46.5 | 46.1 | 45.8 | 45.8 | 46.5 | 45.7 |
| Error | 2.1 | 2.5 | 2.2 | 2.9 | 2.5 | 2.2 | 2.2 | 2.9 | 2.1 |

| Bridge deck | Precise level/mm | Average error/mm | Accuracy |
|---|---|---|---|
| Left pavement | 44.6 | 2.3 | 5.18% |
| Error | | | |
| Right pavement | 43.6 | 2.4 | 5.57% |
| Error | | | |

As shown in Figure 8, both the left and right sides of the main bridge are deformed asymmetrically. Compared to the points in the midspan of the main bridge, the points near the west bank have the largest relative deformation 66.49mm and 66.15mm. This is because the arch column on Daning River Bridge is steel bent structure, and the general structure is as shown in Figure 9a. Due to the terrain where Daning river bridge located is high in the west and low in the east, the length of the column of the west half span arch is larger than that of the corresponding east span arch. The distribution and length of the columns on the arch are shown in Figure 9b. Under the same heating condition, the longer column will produce more elongation, while the stiffness of the arch ring is greater than the box girder. Therefore, the linear expansion of the column rises along the column axis and acts on the upper box girder, resulting in uneven deformation of the bridge deck.

The surface deformation measurement method based on NURBS surface control points is adopted to analyze the deformation of the arch ring of Daning River

Bridge. The point cloud data of top and bottom chords of the arch ring before and after deformation are extracted to construct the displacement function $D(u, v)$. The local shape change of top and bottom chords under the temperature rise is shown in Figure 10, and the curve represents the continuously relative deformation of the top and bottom chords. To verify the accuracy, the sectional displacement functions of the top and bottom chords are solved at the interval of 10-15m, and the relative deformation of the cross section is marked with an equal geometric line.

As shown in Figure 10, under the temperature rise effect, the largest relative deformations of the top chord and the bottom chord are about 45.6mm and 44.3mm, respectively. The point near the vault has the maximum relative deformation. Besides the arch foot, the arch ring presents an overall uplift trend. In order to verify the accuracy of large span bridge deformation measurement method based on three-dimensional laser scanning point cloud data, the deformation of arch ring is measured by total station. The measuring points are arranged in accordance with the deformation section solved in Figure 10. The deformation measurement of the NURBS surface control point are compared with the total station measurement, as shown in Table 2. The accuracy of the measurement of NURBS surface control point can be basically controlled within 5%. The high measuring accuracy can accurately reflect the overall deformation of load-bearing components of large span bridges.

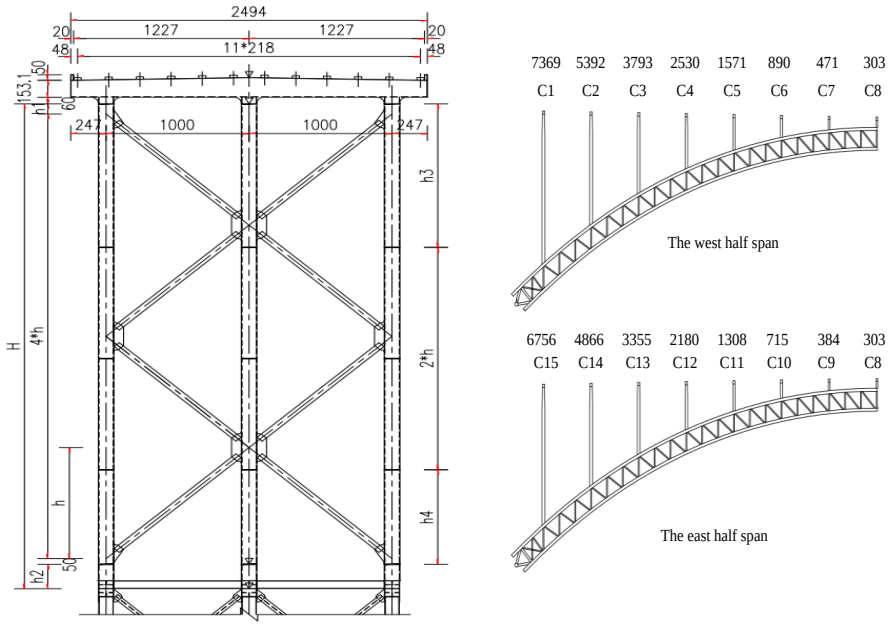


(a) Column structure drawing (cm)

(b) Value of length of arch column(mm)

*Figure 9. Layout and construction drawing of column on arch*

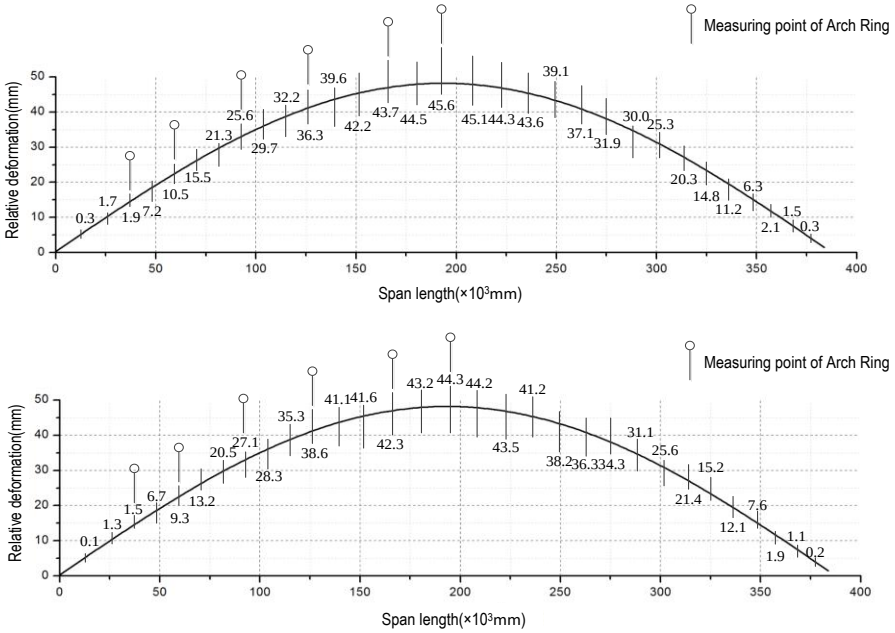


*Figure 10. Relative deformation of the top and bottom chords*

*Table 2. Deformation value of arch ring*

| | | | | | | |
|---|---|---|---|---|---|---|
| Top chord of arch ring | Total station measurement value/mm | | | | | |
| | 1.8 | 10.1 | 24.3 | 37.5 | 42.5 | 44.2 |
| | Integral deformation measurement value/mm | | | | | |
| | 1.9 | 10.5 | 25.6 | 36.3 | 43.7 | 45.6 |
| Error | 0.1 | 0.4 | 1.3 | 1.2 | 1.2 | 1.4 |
| Accuracy | 5.56% | 3.96% | 5.34% | 3.20% | 2.82% | 3.17% |
| Bottom chord of arch ring | Total station measurement value/mm | | | | | |
| | 1.5 | 9.0 | 26.3 | 37.1 | 40.7 | 42.8 |
| | Integral deformation measurement value/mm | | | | | |
| | 1.5 | 9.3 | 27.1 | 38.6 | 42.3 | 44.3 |
| Error | 0 | 0.3 | 0.8 | 1.5 | 1.6 | 1.5 |
| Accuracy | - | 3.33% | 3.04% | 4.03% | 3.93% | 3.50% |

## 4. Conclusions

In this paper, a large-span bridge deformation monitoring method by three-dimensional laser scanning system is proposed and successfully implemented. The following conclusions are drawn:

(1) Considering the precision of three-dimensional laser scanning point cloud data, a layout scheme of long span bridge measurement points based on point cloud precision distribution is proposed. The layout of the measuring points under this scheme is simple and the number of measurement stations is small enough to facilitate the scanning of large span bridges. Moreover, the scheme has other advantages like broad coverage, high repetition rate of high density point cloud, and precise 3D point cloud data.

(2) A new deformation measurement method for bridge NURBS surface based on 3D point cloud data is proposed. The deformed surface is represented as a synthetic surface of NURBS original surface and displacement function. The surface deformation is independent of the control mesh, and the key points can be selected at random. The deformation results can be obtained directly by solving the displacement function D (u, v), and the surface deformation of the bridge can be obtained.

(3) By comparing the measurement results between total station and precision level, the surface deformation measurement method based on NURBS surface control point can accurately reflect the overall deformation and linear deformation of long-span bridge. Its measurement error is within 5%, which has a good prospect in engineering application.

*Acknowledgment*

*This paper was supported by the National Nature Science Foundation of China (51778094, 51708068).*

## References

Battauz M., Bellio R., Gori E. (2011). Covariate measurement error adjustment for multilevel models with application to educational data. *Journal of Educational & Behavioral Statistics*, Vol. 36, No. 3, pp. 283-306. http://dx.doi.org/10.3102/1076998610366262

Bergström P. (2015). Evaluation of NURBS surfaces for regular structured parameter values. *Journal of Computing & Information Science in Engineering*, Vol. 15, No. 1, pp. 13-21. http://dx.doi.org/10.1115/1.4028956

Chen M. G., Chen C. S., Wu C. T. (2010). Monitoring of sag deformation in suspension bridges using a 3D laser scanner. *Circulation Research*, Vol. 115, No. 5, pp. 475-479.

Cristea C., Jocea A. F. (2015). Applications of terrestrial laser scanning and GIS in forest inventory. *Journal of Applied Engineering Sciences*, Vol. 5, No. 2, pp. 13-20. http://dx.doi.org/10.1515/jaes-2015-0016

Du J. C., Teng H. C. (2007). 3D laser scanning and GPS technology for landslide earthwork volume estimation. *Automation in Construction*, Vol. 16, No. 5, pp. 657-663. http://dx.doi.org/10.1016/j.autcon.2006.11.002

Gonzálezferreiro E., Diéguezaranda U., Barreirofernández L. (2013). A mixed pixel- and region-based approach for using airborne laser scanning data for individual tree crown delineation in D. Don plantations. *International Journal of Remote Sensing*, Vol. 34, No. 21, pp. 7671-7690. http://dx.doi.org/10.1080/01431161.2013.823523

Leonidopoulos G. (2016). Modelling and simulation of electric power transmission line current as wave. *Modelling, Measurement and Control A*, Vol. 89, No. 1, pp. 1-12.

Nurunnabi A., Belton D., West G. (2016). Robust segmentation for large volumes of laser scanning three-dimensional point cloud data. *IEEE Transactions on Geoscience & Remote Sensing*, Vol. 54, No. 8, pp. 4790-4805. http://dx.doi.org/10.1109/TGRS.2016.2551546

Riveiro B., Morer P., Arias P. (2011). Terrestrial laser scanning and limit analysis of masonry arch bridges. *Construction & Building Materials*, Vol. 25, No. 4, pp. 1726-1735. http://dx.doi.org/10.1016/j.conbuildmat.2010.11.094

Soni A., Robson S., Gleeson B. (2015). Structural monitoring for the rail industry using conventional survey, laser scanning and photogrammetry. *Applied Geomatics*, Vol. 7, No. 2, pp. 1-16. http://dx.doi.org/10.1007/s12518-015-0156-1

Wyvill G., Cao E., Trotman A. (1992). The Cao En surface: A new approach to freeform geometric models. *Programming & Computer Software*, Vol. 18, No. 4, pp. 31-40.

Zawieska D., Markiewicz J. (2015). Utilisation of laser scanning technology and digital images for measurements of industrial objects - A case study. *Reports on Geodesy & Geoinformatics*, Vol. 98, No. 1, pp. 28-38. http://dx.doi.org/10.2478/rgg-2015-0003

Zeng K., Jiang Y. (2015). Application of 3D laser scanning technology in surface subsidence monitoring. *Surveying and Mapping of Geology and Mineral Resources*, Vol. 13, No. 2, pp. 13-18. http://dx.doi.org/10.3969/j.issn.1007-9394.2015.02.008

Zhang F., Sun, K. (2016). Tensorial biometric signal recognition based on multilinear PCA plus GTDA. *Advances in Modelling and Analysis B*, Vol. 59, No. 1, pp. 91-112. http://dx.doi.org/10.1007/978-3-662-49014-3_54

Zhou H., Zhu D., Qu H. (2011). The application of 3D laser scanning technology and GIS in ancient architecture protection. *Geotechnical Investigation & Surveying*, Vol. 39, No. 6, 73-77.